Performance Evaluation of a Permanent Magnet Electric-Drive-Reconfigured Onboard Charger with Active Power Factor Correction

Feng Yu, *Member, IEEE*, Zhihao Zhu, Jingfeng Mao, and Juping Gu
(Invited)

***Abstract*—This paper presents a comprehensive charging operation for an electric-drive-reconfigured onboard charger (EDROC) with active power factor correction (APFC). The charging topology exclusively utilizes the three-phase permanent magnet synchronous motor (PMSM) propulsion system as a three-channel boost-type converter in which only a contactor and a small diode bridge are added. First, the operation scenario of the EDROC is introduced. Second, the relationship between electromagnetic torque and rotor position is investigated. Third, the current ripple cancellation of the EDROC is discussed in detail. Moreover, to implement the single-phase APFC along with charging voltage/current regulation of propulsion battery, control strategies including current balancing and synchronous/interleaving PWM strategies are incorporated. Finally, 200W proof-of-concept prototype-based tests are conducted under different operation scenarios.**

***Index Terms*—Active power factor correction, current balancing, electric-drive-reconfigured, electromagnetic torque, interleaving, onboard charger.**

I. Introduction

With further concerning of environmental issues, research on electric vehicle (EV) has attracted sustained attention during last three decades [1]-[2]. The main electrical equipment of EV consists of battery charger and propulsion system. Generally, the battery charger is classified into onboard charger and offboard charger [3]-[5]. Although the offboard charger is capable of high-power fast charging, the geographical density is relatively low. Comparatively, onboard charger can be considered as a promising supplement over its offboard counterpart.

Traditionally, an independent onboard battery charger is bulky and expensive, which will significantly add cost, volume, and weight to the EVs. In general, the propulsion motor and the inverter are never engaged when propulsion battery is being charged. Thus, electric-drive-reconfigured onboard charger (EDROC) has been viewed as a promising solution in addressing the weight, volume, and cost considerations of battery charger [6]. Hence numerous EDROC topologies have been proposed during the last few decades, which involve an extensive range of motor types, converter topologies, and power levels [7]-[10].

In particular, according to the post-reconfigured function of the propulsion motor stator windings, the EDROC can be categorized into two types, namely, the filter inductor (FI) type [11]-[12] and the energy storage inductor (ESI) type [13]-[15]. Most of the existing research focus on the FI reconfiguration manner where the propulsion inverter legs are reconfigured as a pulse width-modulated (PWM) voltage source rectifier and that is directly connected to the utility grid through motor stator windings. However, the EDROC may suffer from the problem of non-zero electromagnetic torque generation, due to the alternating currents flowing through the motor stator windings as discussed in [16], [17]. In addition, extra components require to be installed on the EVs to establish an electromagnetic interference filter or to eliminate the electromagnetic torque [18]. Comparatively, the control strategies concerning the sinusoidal input currents are relatively complicated.

Other group of efforts have been focused on the ESI reconfiguration manner where the propulsion inverter is reconfigured as the DC/DC converter, while the motor stator windings are reutilized as ESIs. However, the current research has mainly focused on the structure, operation principles, and the battery charging current ripple. In [19], a typical of EDROC is introduced, where an additional single-phase diode bride rectifier is employed to connect to the neutral point of the propulsion motor, and the propulsion inverter and motor stator windings are reutilized to boost the rectifier output voltage. To reduce the ripples in the input current for better total harmonic distortion (THD) performance, interleaved PWM strategy is adopted in [19]-[21]. However, when compared to the synchronous PWM strategy, the interleaved PWM strategy yields higher phase currents ripples as discussed in [22], [23]. In [23], to compensate the small common mode inductance that inherently exists in the motor stator winding, additional boost inductors are installed between the utility grid and the neural point of the propulsion motor. Previous work has confirmed that instantaneous zero electromagnetic torque can be realized in terms of this configuration. However, when a permanent magnet

Manuscript was submitted for review on 30, January, 2019.
This work was supported in part by the National Natural Science Foundation of China (51807098、61673226) and the Six Talent Peaks Project in Jiangsu Province (2015-JY-028).
Feng Yu, Zhihao Zhu, Jingfeng Mao and Juping Gu are with the School of Electrical Engineering, Nantong University, Nantong 226019, China (e-mail: yufeng628@ntu.edu.cn, 17805058432@163.com, mao.jf@ntu.edu.cn, gu.jp@ntu.edu.cn).
Digital Object Identifier 10.30941/CESTEMS.2019.00010

synchronous motor (PMSM) is incorporated in the EDROC system, the motor may rotate a certain angle and then at standstill in case imbalance phase currents flow through the motor stator windings during the charging process, due to the interaction between the stator flux and rotor permanent magnet (PM) flux which inherently exists in the propulsion motor. Hence, zero electromagnetic torque should be ensured when charging mode is activated especially under the imbalance current excitation.

In this paper, an EDROC evolved from a three-phase permanent magnet propulsion system already installed in the EV is studied, and comprehensive performance evaluations are conducted with active power factor correction (APFC). The key contributions of this paper are: (1) the relationship between electromagnetic torque and rotor position is obtained based on magnetic energy; and (2) three-channel APFC along with synchronous/interleaving PWM strategy is implemented in the EDROC system. In Section II, the topology structure and operation principle are analyzed in detail. Investigation of electromagnetic torque production associated with rotor position is given in Section III. Control algorithms are provided in Section IV. In Section V, a 200W proof-of-concept prototype is built up. Finally, conclusions are made in Section VI.

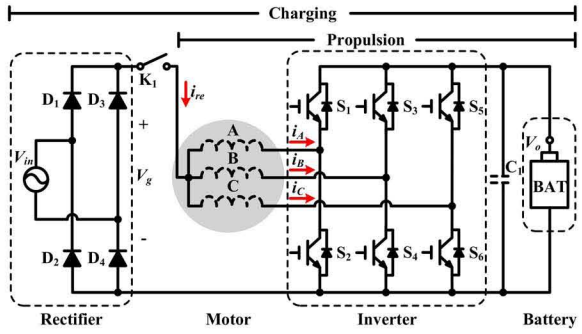

Fig. 1. Topology structure of the EDROC system.

II. Operation Principle of The EDROC System

Fig 1 illustrates the EDROC topology structure, in which the power components have already been installed in EVs, such as a three-phase PMSM, an inverter and so on. It should be noticed that extra power components are not required other than a contactor and a rectifier.

In propulsion mode, the connector K_1 is opened. Firstly, the energy of the propulsion battery is converted into the electric energy for driving PMSM through inverter. Then, the electric energy for driving PMSM is converted into mechanical energy for driving EV. In this mode, the additional rectifier has no effect on the propulsion system.

In charging mode, the connector K_1 is closed. The rectifier is utilized to rectify input AC line voltage, while the motor stator windings along with the inverter are reconfigured a three-channel boost-type converter, which is employed to regulate the charging voltage/current. Meanwhile, the motor stator windings are reutilized as ESIs as discussed in Section I.

Fig. 2 demonstrates the eight operation modes of the EDROC system. In charging period, switches S_1, S_3, and S_5 are always turned OFF, and switches S_2, S_4, and S_6 have the same switching frequency in view of acceptable electromagnetic interference. In mode I, the switches S_2, S_4, and S_6 are turned OFF, while the antiparallel diodes of S_1, S_3, and S5 conduct. The voltages across motor stator windings A, B, and C, are equal to V_g-V_o. Switches states and correlation voltages for each mode of operation are listed in Table I.

TABLE I
SWITCHES STATES AND CORRELATION VOLTAGES for EACH MODE of OPERATION

	Mode I	Mode II	Mode III	Mode IV
Propulsion system	S_2 OFF	S_2 ON	S_2 OFF	S_2 OFF
	S_4 OFF	S_4 OFF	S_4 ON	S_4 OFF
	S_6 OFF	S_6 OFF	S_6 OFF	S_6 ON
Voltage over A	V_g-V_o	V_g	V_g-V_o	V_g-V_o
Voltage over B	V_g-V_o	V_g-V_o	V_g	V_g-V_o
Voltage over C	V_g-V_o	V_g-V_o	V_g-V_o	V_g
	Mode V	Mode VI	Mode VII	Mode VIII
Propulsion system	S_2 ON	S_2 ON	S_2 OFF	S_2 ON
	S_4 ON	S_4 OFF	S_4 ON	S_4 ON
	S_6 OFF	S_6 ON	S_6 ON	S_6 ON
Voltage over A	V_g	V_g	V_g-V_o	V_g
Voltage over B	V_g	V_g-V_o	V_g	V_g
Voltage over C	V_g-V_o	V_g	V_g	V_g

III. Theoretical Analysis

A. Electromagnetic Torque Based on Magnetic Energy

Since PMSMs can offer a higher efficiency and torque density [24], they are considered as promising applications in EVs. However, due to the interaction between the stator flux and rotor PM flux which inherently exists in the PMSMs, electromagnetic torque may be produced when the charging currents flow though the motor stator windings. Non-negligible torque will cause the movement, which is strictly prohibited in the charging process. Hence, the assessment of the electromagnetic torque should be reasonably conducted.

Although the electromagnet torque can be easily estimated by the Park transformation theory, the average rather than instantaneous value can be obtained in this conventional way. Nevertheless, the rotor may rotate at a certain rotor position no matter whether AC or DC currents flow through the motor stator windings [25]. For the sake of simplicity, the electromagnetic torque is thus evaluated according to magnetic energy (W_m).

Assume that there are n (n=1,2,3,…) sets of windings on the stator and a rotor that outputs mechanical energy in the motor, if the flux linkages of n windings ψ_1, ..., and ψ_n and rotor angle θ_e (electric angle) serve as the independent variables, W_m can be expressed as

$$W_m = \int_0^{\psi_1} i_1\left(\psi_1', 0, \ldots, 0, \theta_e\right) d\psi_1' + \int_0^{\psi_2} i_2\left(\psi_1, \psi_2', 0, \ldots, 0, \theta_e\right) d\psi_2' + \ldots + \int_0^{\psi_n} i_n\left(\psi_1, \psi_2, \ldots, \psi_n', \theta_e\right) d\psi_n' \quad (1)$$

where i_n is the excitation current in the *nth* winding. Assume that the rotor makes a minute imaginary shift $d\theta_{mech}$, the variation of W_m is

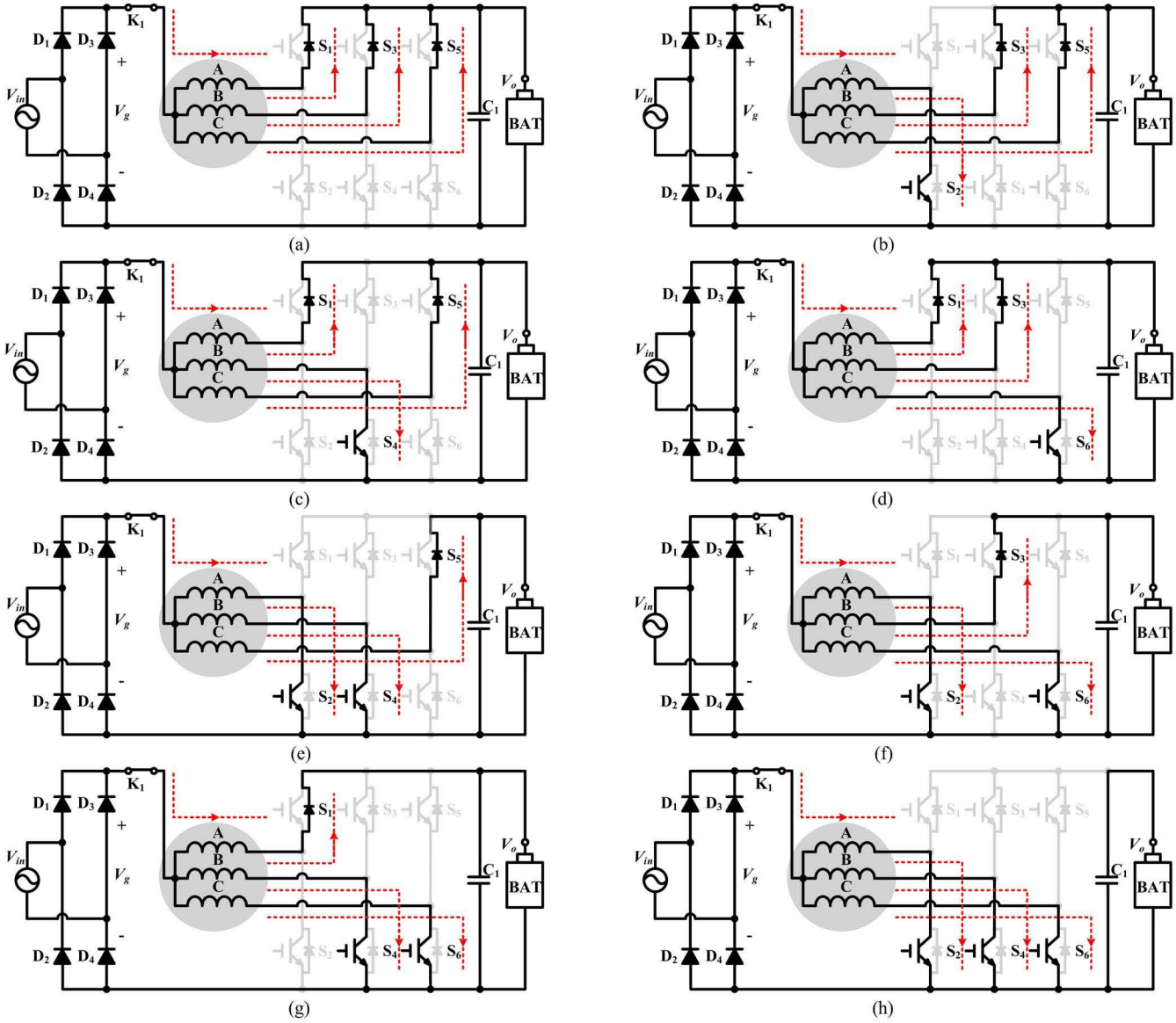

Fig. 2. Operation modes of the EDROC system. (a) Mode I. (b) Mode II. (c) Mode III. (d) Mode IV. (e) Mode V. (f) Mode VI. (g) Mode VII. (h) Mode VIII.

$$dW_m = \sum_1^n \frac{\partial W_m}{\partial \psi_k} d\psi_k + \frac{\partial W_m}{\partial \theta_{mech}} d\theta_{mech} \tag{2}$$

According to the law of conservation of energy, the input energy from the power source dW_e should be equal to the sum of the increment of W_m and the output mechanical energy dW_{mech}, then dW_m can be denoted as

$$dW_m = dW_e - dW_{mech} = \sum_1^n i_k d\psi_k - T_e d\theta_{mech} \tag{3}$$

where T_e represents electromagnetic torque; θ_{mech} represents mechanical angle, which follows $\theta_{mech}=\theta_e/n_p$; and n_p denotes the number of pole pairs. Thus, combining (2) and (3) it can be found that

$$\begin{cases} T_e = -\dfrac{\partial W_m}{\partial \theta_{mech}} \\ \dfrac{\partial W_m}{\partial \psi_k} = i_k \end{cases} \tag{4}$$

From (4), it is indicated that the rotor will produce a certain amount of electromagnetic torque when the deviation of magnetic energy occurs, which is caused by a tiny virtual shift of the rotor.

Supposing that the magnetic road is linear and PMSM is adopted, the magnetic energy in (1) can be renewed as

$$\begin{aligned} W_m = {} & \frac{1}{2}L_{11}(\theta)i_1^2 + \frac{1}{2}L_{22}(\theta)i_2^2 + \ldots + \frac{1}{2}L_{nn}(\theta)i_n^2 + L_{12}(\theta)i_1 i_2 + \\ & W_r + L_{13}(\theta)i_1 i_3 + \ldots + L_{(n-1)n}(\theta)i_{n-1} i_n + i_1\psi_{fd}\cos(\theta) + \\ & i_2\psi_{fd}\cos(\theta - \frac{2\pi}{n}) + \ldots + i_n\psi_{fd}\cos(\theta - \frac{2(n-1)\pi}{n}) \end{aligned} \tag{5}$$

where W_r is the magnetic energy produced by PMs and it is not associated with the rotor position and currents flowing through motor stator windings; ψ_{fd} is the maximum flux linkage that the PM flux linkage produces in stator winding; $L_{11}(\theta)$, ..., and $L_{nn}(\theta)$ are the stator self-inductances; $L_{12}(\theta)$, $L_{13}(\theta)$, ..., and $L_{(n\text{-}1)n}(\theta)$ are the stator mutual inductances.

Thus, the electromagnetic torque generated by a three-phase PMSM can be expressed as

$$T_e = -\frac{\partial W_m}{\partial \theta_{mech}} = -n_p \frac{\partial W_m}{\partial \theta_e} = -n_p \left[\mathbf{i}_s^T \psi_{fd} \frac{\partial \xi}{\partial \theta_e} + \frac{1}{2} \mathbf{i}_s^T \frac{\partial \mathbf{L}_s}{\partial \theta_e} \mathbf{i}_s \right] \quad (6)$$

where $\xi=[\cos(\theta_e)\ \cos(\theta_e-2\pi/3)\ \cos(\theta_e-4\pi/3)]^T$; $\mathbf{i}_s=[i_A\ i_B\ i_C]^T$; and $\mathbf{L}_s$ is the motor inductance matrix, which can be represented as

$$\mathbf{L}_s = \begin{bmatrix} L_{AA} & L_{AB} & L_{AC} \\ L_{BA} & L_{BB} & L_{BC} \\ L_{CA} & L_{CB} & L_{CC} \end{bmatrix} \quad (7)$$

Moreover, the stator self-inductances and the stator mutual inductances in the three-phase PMSM can be represented as

$$\begin{cases} L_{AA} = L_{s\sigma} + L_{s0} + L_{S1}\cos(2\theta_e) \\ L_{BB} = L_{s\sigma} + L_{s0} + L_{S1}\cos\left(2\theta_e - \frac{2}{3}\pi\right) \\ L_{CC} = L_{s\sigma} + L_{s0} + L_{S1}\cos\left(2\theta_e + \frac{2}{3}\pi\right) \\ L_{AB} = L_{BA} = M_{s0} + M_{s1}\cos\left(2\theta_e - \frac{1}{3}\pi\right) \\ L_{AC} = L_{CA} = M_{s0} + M_{s1}\cos\left(2\theta_e + \frac{1}{3}\pi\right) \\ L_{BC} = L_{CB} = M_{s0} + M_{s1}\cos(2\theta_e + \pi) \end{cases} \quad (8)$$

where $L_{S\sigma}$ is the stator phase winding leakage inductance; L_{mq} is the q-axis inductance component; L_{md} is the d-axis inductance component; $L_{s0}=1/2(L_{mq}+L_{md})$; $L_{s1}=1/2(L_{mq}-L_{md})$; $M_{s0}=-1/2L_{s0}=-1/4(L_{mq}+L_{md})$; $M_{s1}=-1/2L_{s1}=-1/4(L_{mq}-L_{md})$.

Once $\mathbf{i}_s$, L_{md}, L_{mq}, and ψ_{fd} are measured and identified, the electromagnetic torque can be calculated in terms of the rotor position according to (6). Consequently, the zero electromagnetic torque can be achieved at a specific rotor position when zeroing the equation (6). For example, if imbalance current flow through phases A, B, C, i.e., $i_A=i_B=2i_C$, the rotor position that yields the zero electromagnetic torque can be determined as

$$\theta_e = \frac{1}{3}\pi \ \text{ or } \ \theta_e = \frac{4}{3}\pi \quad (9)$$

As such, the propulsion motor rotor must be parked in a specific position before charging, while it is very inconvenient in practical operation. Fortunately, it should be noted that when the charging currents in the stator phase windings are kept the same, i.e., $i_A=i_B=i_C$, electromagnetic torque is theoretically up to zero no matter where the rotor parks, which is in accordance with practical charging scenario.

B. Currents Ripples in The EDROC System

In particular, the currents ripples should also be concerned in the charging process. Fortunately, the EDROC system can be considered as a typical three-channel boost-type converter as discussed in Section II. Due to the symmetry of the motor structure, it is assumed that the equivalent phase inductances in the motor stator are equal, i.e., $L_A=L_B=L_C$. On this basis, the steady-state operation of the EDROC system can be divided into three kinds of operation modes in the continuous conduction mode, especially when the duty cycle (D) is incorporated in the bottom switches, the following relations can be obtained as: (1) $0<D<1/3$, in which $V_g<V_o<3/2V_g$; (2) $1/3<D<2/3$, in which $3/2V_g<V_o<3V_g$; and (3)$2/3<D<1$, in which $V_o>3V_g$.

It can be seen from Fig. 3(a) that if $0<D<1/3$, the EDROC system operates in a periodic sequence of (II)-(I)-(III)-(I)-(IV)-(I)-(II). Obviously, due to the same switching pattern, the input currents ripples are equal in mode II-IV, and their absolute values are theoretically equivalent to the one in mode I. Meanwhile, according to the Kirchhoff's voltage law, the mathematic model in mode I can be expressed as

$$\begin{cases} L_A \frac{di_1}{dt} = V_g - V_o = \frac{-D}{1-D} V_g \\ L_B \frac{di_2}{dt} = V_g - V_o = \frac{-D}{1-D} V_g \\ L_C \frac{di_3}{dt} = V_g - V_o = \frac{-D}{1-D} V_g \end{cases} \quad (10)$$

Due to the fact that the input current i_{in} is the sum of the phase currents ($i_A+i_B+i_C$), the absolute value of the current ripple Δi_{in} in the condition of $0<D<1/3$ can be calculated as

$$|\Delta i_{in}| = |\Delta i_1 + \Delta i_2 + \Delta i_3| = \frac{V_g}{L_A f} \frac{D-3D^2}{1-D} \quad (11)$$

where f is the switching frequency.

Similarly, for $1/3<D<2/3$ and $2/3<D<1$, $|\Delta i_{in}|$ can be represented as (12) and (13), respectively.

$$|\Delta i_{in}| = |\Delta i_1 + \Delta i_2 + \Delta i_3| = \frac{V_g}{L_A f} \frac{-9D^2+9D-2}{3-3D} \quad (12)$$

$$|\Delta i_{in}| = |\Delta i_1 + \Delta i_2 + \Delta i_3| = \frac{V_g}{L_A f}(3D-2) \quad (13)$$

According to (11), (12), and (13), it is found that the input current ripple $|\Delta i_{in}|$ is inversely proportional to the equivalent stator phase inductance and switching frequency. Thereafter, the validity of ripple elimination can be expressed as standardized input current ripple $F(D)$ as

$$F(D) = \frac{|\Delta i_{in}|}{|\Delta i_{A,B,C}|} = \begin{cases} \frac{1-3D}{1-D} & 0 \le D < \frac{1}{3} \\ \frac{(3D-1)(2-3D)}{3D(1-D)} & \frac{1}{3} \le D < \frac{2}{3} \\ \frac{3D-2}{D} & \frac{2}{3} \le D < 1 \end{cases} \quad (14)$$

Similarly, the standardized input current ripple $F(D)$ in a two-channel interleaved boost-type converter, can be obtained as

$$F(D) = \frac{|\Delta i_{in}|}{|\Delta i_L|} = \begin{cases} \frac{1-2D}{1-D} & 0 \le D < \frac{1}{2} \\ \frac{2D-1}{D} & \frac{1}{2} \le D < 1 \end{cases} \quad (15)$$

Fig. 4 illustrates the standardized input currents ripples. Due to the cancellation effect, the interleaved boost-type converters can greatly eliminate the input current ripple. For the EDROC

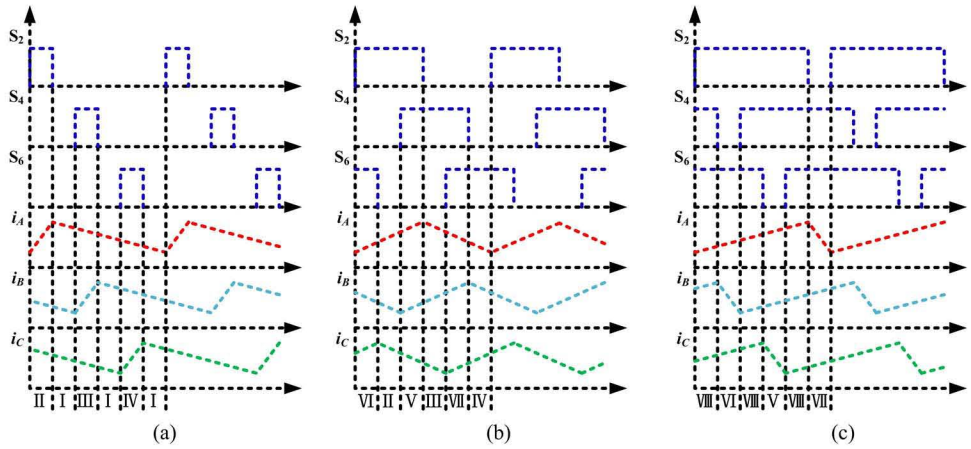

Fig. 3. The current waveforms of the EDROC system during charging. (a) 0<*D*<1/3. (b) 1/3<*D*<2/3. (c) 2/3<*D*<1.

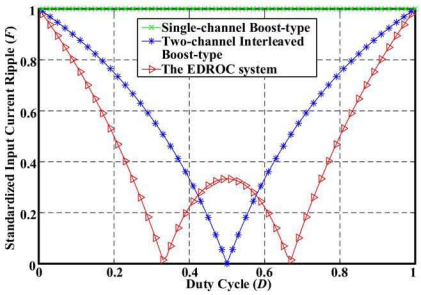

Fig. 4. Standardized input currents ripples for a single-channel boost-type converter, a two-channel interleaved boost-type converter, and the EDROC system.

system, the input current ripple can be completely eliminated when *D*=1/3 or *D*=2/3. While for the two-channel interleaved boost-type converter, the input current ripple can be completely eliminated when *D*=1/2. Compared to two-channel boost-type converter, the EDROC system offers a better performance in current ripple cancellation.

IV. Control Algorithm

It should be noticeable that the EVs must be kept at standstill during charging as discussed in Section III. In order to meet this rigorous requirement, electromagnetic torque should be forced to be zero no matter where the EV parks. However, due to the anisotropy of the PMSM, the phase currents flowing through the motor stator windings are usually different when equal phase voltages are activated. Fortunately, this issue can be easily addressed in a manner where the phase currents are equally shared from the input current from the rectifier, termed as i_A=i_B=i_C.

In order to realize unit power factor (UPF) at the rectifier-side and minimize current ripple causing by the PWM, the control strategy incorporated with three-channel interleaved APFC is employed for the EDROC system. Consequently, it can be observed from Fig. 5 that the controller consists of two parts: (1) a charging voltage/current outer loop is employed to achieve the charging voltage/current regulation; (2) an input current inner loop is adopted to realize UPF and current balancing.

For the charging voltage/current regulation, two PI-controllers are employed to track their desired value $V_{o,\mathrm{ref}}$/$i_{o,\mathrm{ref}}$. In particular, if measured charging voltage V_o is less than the maximum of battery charging voltage $V_{o,\mathrm{ref}}$, the EDROC system will operate in the constant current (CC) charging mode. Once V_o reaches $V_{o,\mathrm{ref}}$, upper and lower saturation limits will be activated and the EDROC system will operate in constant voltage (CV) charging mode.

Furthermore, to achieve current balancing, three PI controllers are employed to regulate i_A, i_B, and i_C, respectively. Meanwhile, their desired values i_{ref} are directly obtained from the absolute value of input voltage V_{in} along with the variable g generated by the voltage PI controller. Since the waveforms of the absolute value of V_{in} and i_{ref} are performed in phase, UPF is theoretically achieved. Especially, the interleaved/ synchronous APFC control strategies can be activated, when the shift between the carrier waves is set to 120°/ 0° respectively.

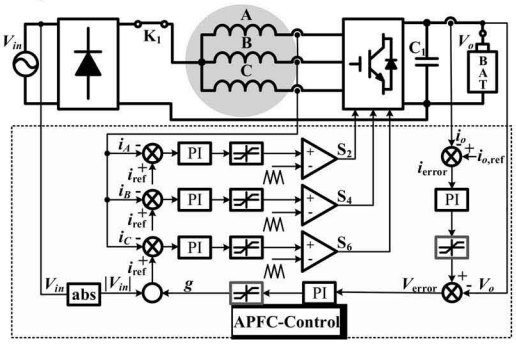

Fig. 5. Control strategy of the EDROC system.

V. Evaluation Results

A. Simulation Results

In order to verify the theoretical results, the EDROC system is tested in terms of the MATLAB/SIMULINK software. The performance evaluations are conducted in the CV charging mode, and the reference value of charging voltage is set to 53V.

First, the simulation with the interleaved APFC control strategy is made. Fig. 6(a) shows the waveforms of input voltage and current. The rms and frequency of input voltage are 40V and 50Hz, respectively. Meanwhile, the current waveform can track the voltage waveform well. As a result,

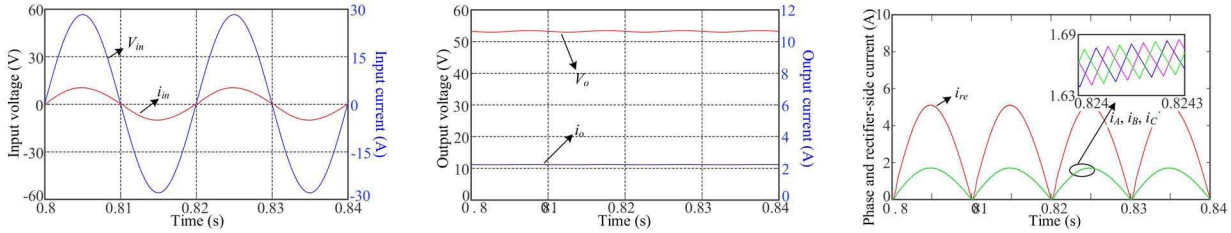

Fig. 6. Simulation evaluation of the EDROC system with the interleaved APFC control strategy. (a) Input voltage and current. (b) Charging voltage and current. (c) Phase and rectifier-side currents.

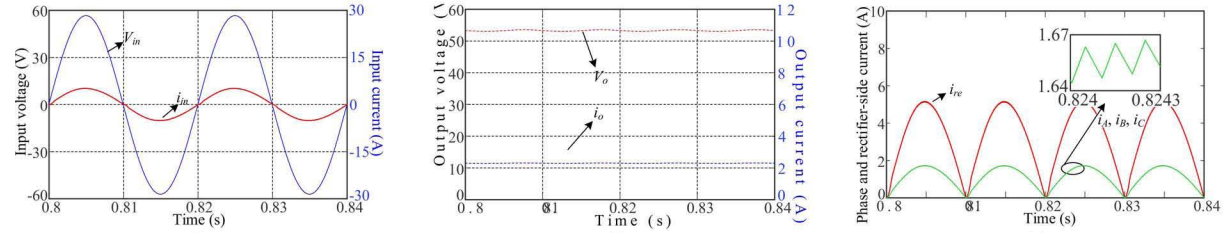

Fig. 7. Simulation evaluation of the EDROC system with the synchronous APFC control strategy. (a) Input voltage and current. (b) Charging voltage and current. (c) Phase and rectifier-side currents.

the UPF can be realized. The charging voltage and current are shown in Fig. 6(b), respectively. It can be observed that the charging voltage is well kept at 53 V and the charging current is 2.3A, which is suitable for battery charging. At the same time, due to mutual compensation of currents ripples in phases A, B, and C, the rectifier-side output current is relatively smooth as illustrated in Fig. 6(c). Additionally, from Fig. 6(c) it can be found that rectifier-side current is 5.1A and the phase currents are same (1.7A), thereby the current balancing is realized.

As a comparison, the simulation of the EDROC system with the synchronous APFC control strategy is also conducted. Fig. 7(a) illustrates the waveforms of input voltage and current. It can be seen that the input current is strictly in phase with the voltage, which can also ensure the UPF operation. Compared with the interleaved scheme, the control with the synchronous APFC algorithm offers the similar performance in the charging voltage/current regulation and current balancing as shown in Fig. 7(b) and Fig. 7(c). Since the inductances of the motor stator windings are big enough, negligible total harmonic distortion (THD) differential in rectifier-sider current can be observed from the comparison between Fig. 6(c) and Fig. 7(c). However, the ripples of phase currents with the interleaved APFC control strategy (0.04A) are a little larger when compared with the synchronous APFC control strategy (0.02A).

B. Experimental Results

To confirm the theoretical results, a 200W experimental setup is developed as depicted in Fig. 8. To obtain a 40V (rms) single-phase voltage source, a custom-made single-phase inverter is utilized along with a DC power source. Moreover, a three-phase interior permanent magnet motor is reutilized as three ESIs and the three-phase inverter consists of three FF300R12ME4 (Infineon) modules. Besides, a 450V/4700μF explosion-proof capacitor is used to filter charging voltage ripple. Here, it should be mentioned that an active filter is utilized in front of 450V/4700μF explosion-proof capacitor to compensate the second-order harmonic caused by the single-phase voltage source. Nevertheless, the active filter is beyond the range of this paper and it is not drawn in the picture above. For voltages and currents measurement, ±100V voltage sensors WHV05AS3S6 and ±25A current sensors WHB25LSP3S1 are used. Then, the control algorithm is

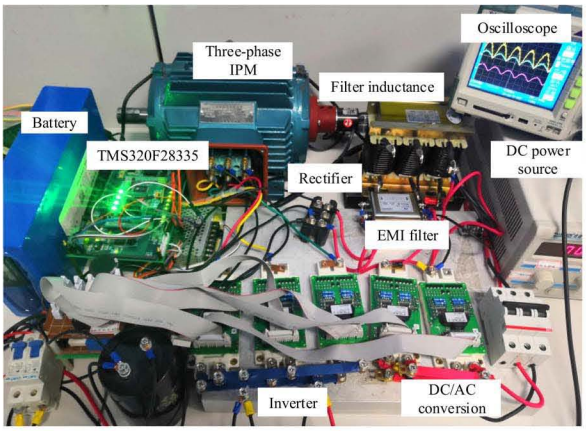

Fig. 8. Experimental setup.

TABLE II
KEY MOTOR PARAMETERS

Parameters	Values
Rated power	2.2kW
Rated frequency	50Hz
Rated speed	1500rpm
No. of pole pairs	2
Phase resistance	5.25Ω
Stator *q*-axis inductance	36mH
Stator *d*-axis inductance	24mH
Stator-PM magnetic flux	0.8Wb

TABLE III
KEY BATTERY PARAMETERS

Parameters	Values
Capacity	20AH
Voltage	48V
Maximum charging current	5A
Maximum output Current	20A
Ceiling voltage	54.6V

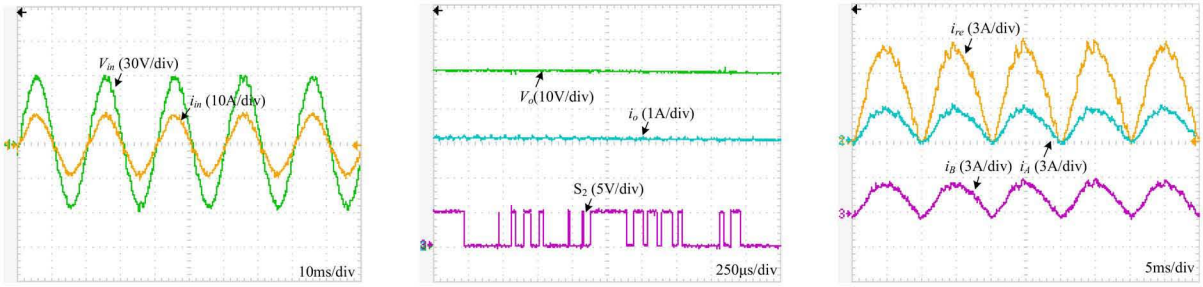

(a) (b) (c)

Fig. 9. Experimental results of the EDROC system with the interleaved APFC control strategy in CC charging mode. (a) Input voltage and current. (b) Charging voltage and current. (c) Phase and rectifier-side currents.

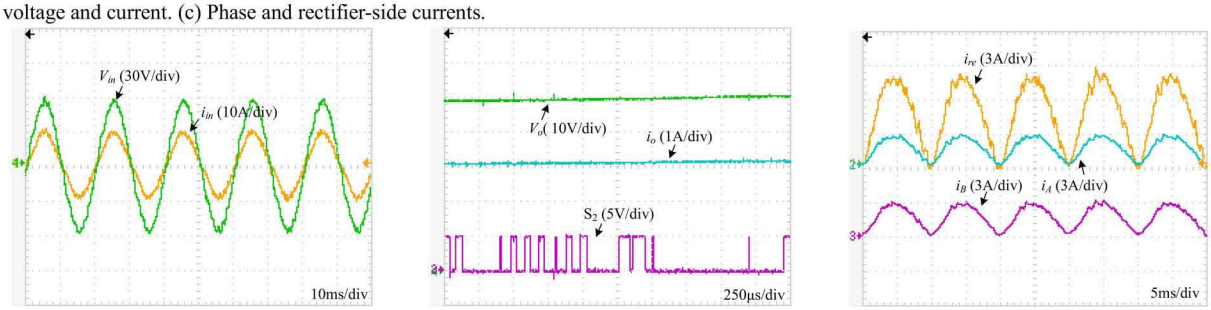

(a) (b) (c)

Fig. 10. Experimental results of the EDROC system with the synchronous APFC control strategy in CC charging mode. (a) Input voltage and current. (b) Charging voltage and current. (c) Phase and rectifier-side currents.

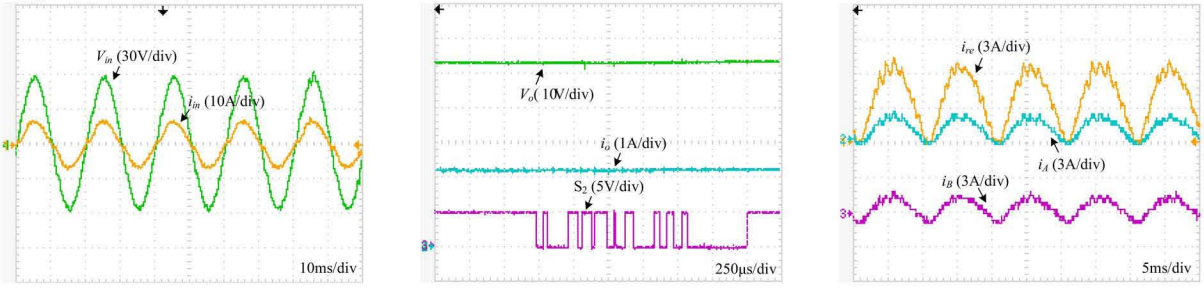

(a) (b) (c)

Fig. 11. Experimental results of the EDROC system with the interleaved APFC control strategy in CV charging mode. (a) Input voltage and current. (b) Charging voltage and current. (c) Phase and rectifier-side currents.

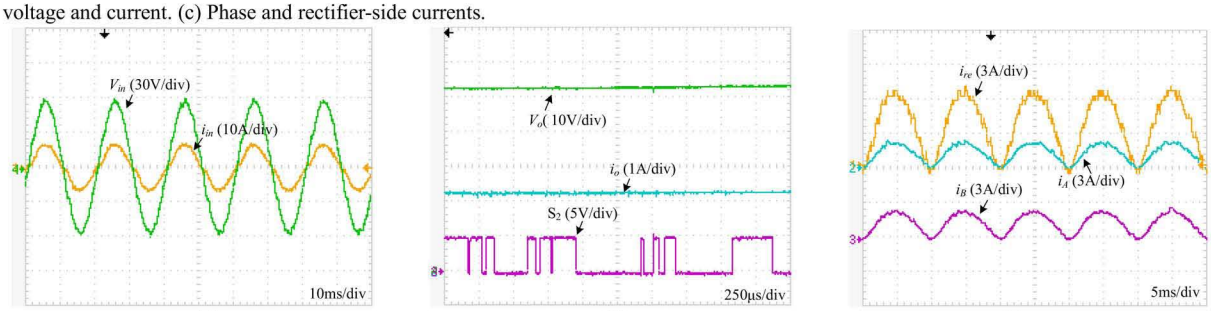

(a) (b) (c)

Fig. 12. Experimental results of the EDROC system with the synchronous APFC control strategy in CV charging mode. (a) Input voltage and current. (b) Charging voltage and current. (c) Phase and rectifier-side currents.

written in the *C* programming language and is implemented by a TMS320F28335 digital controller board.

The key motor parameters and key battery parameters are presented in Table II and Table III, respectively. Moreover, according to the battery parameters, the charging current is set to 3.2A in CC charging mode and the charging voltage is set to 53V in CV charging mode.

Fig. 9 and 10 illustrate the experimental waveforms of the EDROC system with the two APFC control strategies in the CC charging mode. As shown in Fig. 9(a) and 10(a), it can be noted that the phase shift between the input voltage and the input current is negligible, hence the EDROC system can operate at UPF scenario. Moreover, in Fig. 9(b) and 10(b), it can be found that both the charging currents are regulated to 3.2A which is in accordance with the charging requirement. Then, as shown in Fig. 9(c) and Fig. 10(c), although the ripples of phase currents i_A and i_B with the interleaved APFC control strategy (approximately 0.5A) are a little higher, the ripple of the rectifier-side output current i_{re} is relatively smaller, which is consistent with the theoretical analyses in section III. Besides, it can also be observed that i_A and i_B are equal and i_{re} is approximately 8.4A, thus ensuring the zero electromagnetic torque production.

The experimental results of the EDROC system with

synchronous and interleaved APFC control strategies in CV charging mode are shown in Fig. 11 and 12, respectively. From Fig. 11(a) and Fig. 12(a), it can be found that the UPF operation can be achieved with the negligible phase shift between input voltage and current. Furthermore, from Fig. 11(b) and Fig. 12(b), it can be seen that the charging voltages with both two control strategies are well kept at a constant value of 53V. Moreover, the experimental waveforms of i_A, i_B as well as i_{re} are illustrated in Fig. 11(c) and Fig. 12(c). It should be noticeable that the ripple of i_{re} can be effectively reduced when the interleaved control strategy is incorporated (from 0.6A to 0.45A).

On the whole, both the control strategies can achieve the purpose of current balancing, which agrees with the condition of zero electromagnetic torque. However, compared to the synchronous APFC strategy, it can be found that the interleaved APFC control strategy has a better performance in input current ripple. Although the phase currents ripples with the interleaved APFC control strategy are larger than the synchronous APFC, the amplitude of instantaneous torque produced by the phase currents ripples is much smaller than the inertia torque in EVs. Consequently, the interleaved APFC control strategy is more suitable for the EDROC system.

VI. Conclusion

A permanent magnet electric-drive-reconfigured onboard charger (EDROC) with active power factor correction (APFC) for EV is studied. The EDROC topology exclusively utilizes the three-phase PMSM propulsion system as a three-channel boost-type converter, in which only a contactor and a small diode bridge are added. In order to realize the zero electromagnetic torque production in charging mode, the detailed analysis of the relationship between electromagnetic torque and rotor position are explored. Then, to implement the single-phase APFC along with charging voltage/current regulation of propulsion battery, control strategies including current balancing and synchronous/interleaving PWM strategies are incorporated. Finally, to verify the EDROC system, a 200W experimental setup is developed in the laboratory. Both simulation and experiment results demonstrate the validity of the EDROC system.

REFERENCES

[1] K. Rajashekara, "Present status and future trends in electric vehicle propulsion technologies," *IEEE Journal of Emerging and Selected Topics in Power Electronics*, vol. 1, no. 1, pp. 3-10, Mar. 2013.

[2] C. H. Li, X. M. Zhao, and C. L. Liao, "A graphical analysis on compensation designs of large-gap CPT systems for EV charging applications," *CES Transactions on Electrical Machines and Systems*, vol. 2, no. 2, pp. 232-242, Jun. 2018.

[3] M. Yilmaz and P. Krein, "Review of battery charger topologies, charging power levels, and infrastructure for plug-in electric and hybrid vehicles," *IEEE Trans. Power Electron.*, vol. 28, no. 5, pp. 2151-2169, May 2013.

[4] A. Khaligh and S. Dusmez, "Comprehensive topological analysis of conductive and inductive charging solutions for plug-in electric vehicles," *IEEE Trans. Veh. Technol.*, vol. 61, no. 8, pp. 3475-3489, Oct. 2012.

[5] T. H. Liu, Y. Chen, and P. H. Yi, "Integrated battery charger with power factor correction for electric-propulsion systems," *IET Electric Power Applications*, vol. 9, no. 3, pp. 229-238, Mar. 2015.

[6] S. Haghbin, S. Lundmark, and M. Alakula, "Grid-connected integrated battery chargers in vehicle applications: review and new solution," *IEEE Trans. Ind. Electron.*, vol. 60, no. 2, pp. 459-473, Feb. 2013.

[7] L. Solero, "Nonconventional onboard charger for electric vehicle propulsion batteries," *IEEE Trans. Veh. Technol.*, vol. 50, no. 1, pp. 144-149, Jan. 2001.

[8] H. Chang and C. Liaw, "Development of a compact switched-reluctance motor drive for EV propulsion with voltage boosting and PFC charging capabilities," *IEEE Trans. Veh. Technol.*, vol. 58, no. 7, pp. 3198-3215, Sep. 2009.

[9] H. Chang and C. Liaw, "An integrated driving/charging switched reluctance motor drive using three-phase power module," *IEEE Trans. Ind. Electron.*, vol. 58, no. 5, pp. 1763-1775, May 2011.

[10] S. Ali, D. Mascarella, and G. Joos, "Torque elimination for integrated battery charger based on two permanent magnet synchronous motor drives for electric vehicles," *IET Electric Power Applications*, vol. 11, no. 9, pp. 1627-1635, Nov. 2017

[11] S. Mukundan, H. Dhulipati, and C. Lai, "Design and optimization of traction IPMSM with asymmetrical damper bars for integrated charging capability using evolutionary algorithm," *IEEE Trans. Energy Convers.*, vol. 33, no. 4, pp. 2060-2069, Dec. 2018.

[12] I. Subotic, N. Bodo, and E. Levi, "An EV drive-train with integrated fast charging capability," *IEEE Trans. Power Electron.*, vol. 31, no. 2, pp. 1461-1471, Feb. 2016.

[13] Y. H. Hu, X. G. Song, and W. P. Cao, "New SR drive with integrated charging capacity for plug-in hybrid electric vehicles (PHEVs)," *IEEE Trans. Ind. Electron.*, vol. 61, no. 10, pp. 5722-5731, Oct. 2014.

[14] M. Truntič, T. Konjedic, and M. Milanovič, "Control of integrated single-phase PFC charger for EVs," *IET Power Electronics*, vol. 11, no. 11, pp. 1804-1812, Sep. 2018

[15] D. Kim, M. Kim, and B. Lee, "An integrated battery charger with high power density and efficiency for electric vehicles," *IEEE Trans. Power Electron.*, vol. 32, no. 6, pp. 4553-4565, Jun. 2017.

[16] S. Haghbin, S. Lundmark, and M. Alakula, "An isolated high-power integrated charging in electrified-vehicle applications," *IEEE Trans. Veh. Technol.*, vol. 60, no. 9, pp. 4115-4126, Nov. 2011.

[17] S. Haghbin, K. Khan, and S. Zhao, "An integrated 20-kW motor drive and isolated battery charger for plug-in vehicles," *IEEE Trans. Power Electron.*, vol. 28, no. 8, pp. 4013-4029, Aug. 2013.

[18] X. M. Lu, K. Iyer, and K. Mukherjee, "Investigation of integrated charging and discharging incorporating interior permanent magnet machine with damper bars for electric vehicles," *IEEE Trans. Energy Convers.*, vol. 31, no. 1, pp. 260-269, Mar. 2016.

[19] G. Pellegrino, E. Armando, and P. Guglielmi, "An integral battery charger with power factor correction for electric scooter," *IEEE Trans. Power Electron.*, vol. 25, no. 3, pp. 751-759, Mar. 2010.

[20] C. Shi, Y. Tang, and A. Khaligh, "A single-phase integrated onboard battery charger using propulsion system for plug-in electric vehicles," *IEEE Trans. Veh. Technol.*, vol. 66, no. 12, pp. 10899-10910, Dec. 2017.

[21] C. Shi and A. Khaligh, "A two-stage three-phase integrated charger for electric vehicles with dual cascaded control strategy," *IEEE Journal of Emerging and Selected Topics in Power Electronics*, vol. 6, no. 2, pp. 898-909, Jun. 2018.

[22] Y. Xiao, C. H. Liu, and F. Yu, "An integrated on-board EV charger with safe charging operation for three-phase IPM motor," *IEEE Trans. Ind. Electron.*, doi: 10.1109/TIE.2018.2880712.

[23] D. Woo, D. Joo, and B. Lee, "On the feasibility of integrated battery charger utilizing traction motor and inverter in plug-in hybrid electric vehicles," *IEEE Trans. Power Electron.*, vol. 30, no. 12, pp. 7270-7281, Dec. 2015.

[24] C. Lai, K. Iyer, and K. Mukherjee, "Analysis of electromagnetic torque and effective winding inductance in a surface mounted PMSM during integrated battery charging operation," *IEEE Trans. Magn.*, vol. 51, no. 11, pp. 1-4, Nov. 2015.

[25] F. Yu, W. Zhang, and Y. C. Shen, "A nine-phase permanent magnet electric-drive-reconstructed onboard charger for electric vehicle," *IEEE Trans. Energy Convers.*, vol. 33, no. 4, pp. 2091-2101, Dec. 2018.

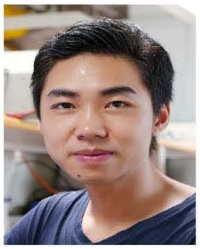

Feng Yu (M'17) was born in Suzhou, China, in 1985. He received the B.Eng. degree in electrical engineering and automation from the School of Electrical Engineering, Sanjiang University, Nanjing, China, in 2008, the M.Sc. degree in electrical engineering from the School of Electrical and Information Engineering, Jiangsu University, Zhenjiang, China, in 2011, and the Ph.D. degree in the electrical engineering in the Department of Electrical Engineering, Southeast University, Nanjing, China, in 2016.

Since 2016, he has been with Nantong University, Nantong, China, where he is currently an Assistant Professor in the School of Electrical Engineering. His current research interests include the control of multiphase machines and drives for applications ranging from automotive to renewable energy.

Zhihao Zhu was born in Henan, China, in 1996. Since 2015, he has been working towards the B.Eng. degree in the School of Electrical Engineering, Nantong University, Nantong, China.

His research interests include battery charging technology and application of power electronics in electric vehicle.

Jingfeng Mao received the B.Eng. degree in industrial automation from the School of Automation, Wuhan University of Technology, Wuhan, China, in 1998. The M. Sc degree and Ph.D. degree both in electric engineering from the School of Electrical and Information Engineering, Jiangsu University, Zhenjiang, China, in 2004 and 2008, respectively.

Since 1998, he has been with Nantong University, Nantong, China, where he is currently a professor in the School of Electrical Engineering. His current research interests include electrical machines and drives, renewable energy generations and applications, control and design of microgrids.

Juping Gu was born in Nantong, China, in 1971. She received the B.Eng. Degree in construction electrical from the School of Automation and Electrical Engineering, Nanjing Tech University, Nanjing, China, in 1992, the M.Sc degree and Ph.D. degree both in electrical engineering from the Department of Electrical Engineering, Southeast University, Nanjing, China, in 1995 and 2003, respectively. She visited the RWTH Aachen University as a visiting professor in 2009.

Since 1995, she has been with Nantong University, Nantong, China, where she is currently the vice-chancellor of Nantong University. Her research interests include the cooperative schedule and control for building groups micro-grid under multiple random disturbances and intelligent measurement and control for the application of equipment manufacturing.